PUNCHING SHEAR RESISTANCE OF FLAT SLABS STRENGTHENED WITH NEAR SURFACE-MOUNTED CFRP BARS

Hikmatullah Akhundzada (Ph.D)[1], Ted Donchev (Ph.D)[2], Diana Petkova (Ph.D)[3]

[1] PhD Student, at Kingston University, Penrhyn Rd, Kingston upon Thames, KT1 2EE, UK. Email: hikmat09@hotmail.com

[2] Associate Professor, at Kingston University, Penrhyn Rd, Kingston upon Thames, KT1 2EE, UK. Email: t.donchev@kingston.ac.uk

[3] Senior Lecturer, at Kingston University, Penrhyn Rd, Kingston upon Thames, KT1 2EE, UK. Email: d.petkova@kingston.ac.uk

ABSTRACT

This paper presents the effectiveness of strengthening slab-column connections against punching shear failure with near-surface mounted (NSM) carbon fibre-reinforced polymer (CFRP) bars. The experimental program consists of preparing and testing eight samples, two control and six strengthened samples. The main variables of the experiment are the strengthening layout and the cross-section area of CFRP bars. The results show that NSM strengthening increases the ultimate load by up to 44%. And the strengthening delays formation of the first crack in concrete thus maintaining a linear behaviour for load-displacement and load-strain curves for higher level of load. The NSM strengthening increases the flexural stiffness by over 100% and maintains a strong bond with concrete throughout the loading. The flexural strength of the slab increases, which subsequently improves the punching shear capacity. The experimental results are compared with several design codes by modification and implementation of Chen & Li's method. There is a good agreement between the calculated ultimate capacity of the strengthened samples and the obtained experimental results.

Keywords: Flat Slabs; Reinforced Concrete; Punching Shear; Strengthening; NSM; CFRP.

INTRODUCTION

With the development of novel materials, the strengthening methods against punching shear failure for flat slabs has evolved over the decades. The traditional methods for increasing the punching shear resistance are: (i) Increasing the depth of the slab; (ii) Post-installation of shear reinforcement; (iii) Enlargement of the column head with concrete; (iv) Enlargement of the column head with a steel structure; and, (v) Increasing the cross-section of the column (Elbakry et.al 2015; Ruiz 2011). Although these techniques are shown to be effective in practice, there are certain limitations such as susceptibility to corrosion, high self-weight, and difficulties in installation. The use of fibre-reinforced polymers (FRP) overcomes these shortcomings and can potentially become a feasible alternative for the current methods.

The existing literature mainly focuses on two methods for strengthening slab against punching shear failure: direct shear strengthening and indirect flexural strengthening. In the flexural strengthening method, FRP materials (sheets, laminates, or bars) are bonded to the tension surface of the slab to act as flexural reinforcement. In the direct shear strengthening method, vertical holes are drilled through the slab. The FRP is placed inside the holes and the cavity is filled with epoxy adhesive to bond the FRP with concrete. These methods enhance the load-carrying capacity of flat slabs by either delaying the punching shear failure or changing the failure mode to flexural or flexural punching.

Externally bonded reinforcement (EBR) is the most commonly used method for strengthening concrete structures with FRP. However, the major disadvantage of FRP EBR strengthening is the premature debonding of the FRP from the surface of the slab (Bilotta et.al 2015). Recently, the researchers are focusing on the use of near-surface mounted (NSM) strengthening of beams and slabs as an alternative to the EBR approach. NSM strengthening method is reported to have many advantages over EBR strengthening such as stronger bond with concrete, protection against accidental impact and higher fire resistance due to embedment of FRP reinforcement in the concrete (De Lorenzis 2007). Bilotta et.al (2015) investigated the efficiency of NSM and EBR flexural strengthening of RC elements. They concluded that the NSM method is less sensitive to debonding and is more effective in increasing the peak-load. Seo et.al (2013) found that the NSM technique exhibits 1.5 times higher bond strength and shows higher magnitude of strain compared to the EBR technique for flexural strengthening of RC beams. An experimental investigation was conducted by Hassan and Rizkalla (2004) for flexural strengthening of RC beams with NSM CFRP bars. The strengthened samples displayed significantly higher ultimate load, yield load, and post-cracking stiffness. The authors proposed a minimum anchorage length of 800 mm and a maximum usable strain of 0.7-0.8% of the CFRP bars.

Agbossou et.al (2008) investigated the effectiveness of strengthening slab-column connections with externally bonded CFRP sheets. They reported increasing the ultimate capacity of the strengthened samples by 15 – 30% which was directly proportional to the number of layers of CFRP strips. Esfahani et.al (2009) investigated the strengthening of interior slab-column connections with CFRP sheets. The strengthened samples displayed higher ultimate capacities compared to the control samples. The improvement due to punching shear strengthening with CFRP sheets was more prominent for slabs made with low amount of steel reinforcement and high strength concrete. In a similar study, Harajli & Soudki (2003) suggested that the punching shear capacity of slab-column connections can be enhanced by up to 45%. The efficiency of the strengthened specimen could further improved by increasing the width of CFRP strips. Similarly, Faraghaly & Ueda (2011) concluded that the punching shear capacity of slabs could be increased by up to 40% with EBR CFRP sheets. Increasing the width of CFRP sheets directly enhanced the ultimate capacities of the strengthened specimens. Akhundzada et.al (2019) found that the use of non-bolted transverse anchorages delayed the debonding of CFRP laminates which subsequently increased the punching shear capacity. The anchorages retain over 90% of the residual strength after reaching their peak load. In a similar study, Akhundzada et.al (2018) proposed that the orthogonal positioning of the CFRP laminates is more efficient compared to diagonal positioning of the laminates for enhancing the punching shear capacity of flat slabs. Abdullah et.al (2013) investigated the use of prestressed CFRP plates for punching shear strengthening of slabs. The slabs strengthened with prestressed CFRP plates displayed significantly lower ultimate load over non-prestressed slabs. In a similar study, Kim et.al (2010) found that the use of prestressed CFRP plates can improve the punching shear capacity by up to 20%. The difference in their findings could be attributed to different anchorage length, steel reinforcement ratio and positioning of the CFRP plates. In the studies above, the rupture of FRP was not reported and the magnitude of the strain in FRP was low. El-Salakawy et. Al (2004) studied the punching shear behaviour of edge column retrofitted with CFRP and GFRP sheets. Some of the slabs were additionally retrofitted with steel bolts acting as shear reinforcement. The samples without shear bolts failed in punching shear while the samples with shear bolts failed in flexure. The samples with flexural CFRP and GFRP sheets increased the ultimate load by up to 23% while the samples with additional shear bolts increased the ultimate load by up to 30%. Chen & Li (2004) investigated the influence of flat slabs with bi-directional GFRP sheets. They found that the ultimate load can be improved by up to 45% and 95% when using single-layer and double-layer GFRP sheets, respectively.

Abdul-Kareem (2019) studied the punching shear strengthening of slab-column connections with the EBR and NSM method. The NSM CFRP reinforcement had a square shape and was positioned in the tension surface of the slab, around the vicinity of the column in orthogonal and skewed configuration. The authors concluded the NSM strengthening method is twice more efficient in increasing the punching shear capacity compared to the EBR method. Azizi & Talaeitaba (2019) conducted a numerical analysis of strengthening flat slabs with CFRP rebars in grooves (EBRIG) and on grooves (EBROG) method. The punching capacity of the numerical strengthened samples improved by up to 62%. George & Mohan found that the EBROG method with FRP could improve the punching shear capacity of flat slabs by up to 58%.

A significant number of studies have concluded that the direct shear strengthening of flat-slabs against punching shear failure with FRP materials (sheets, strands, rods and bolts) is highly efficient and can change the failure mode from punching to flexural or flexural punching (Binici

& Bayrak 2005; Sissakis & Sheikh 2007; Erdogan et.al 2010; Lawler & Polak 2011; Meisami et.al 2013; Meisami et.al 2015; Koppitz et al., 2014).

This research aims to experimentally investigate the efficiency of the NSM method to strengthen slab-column connection against punching shear failure. The two main variables of this study are: the strengthening layout and the cross-sectional area of CFRP bars. The experimental results are analysed and compared with the predictions of the design codes based on the development of analytical modelling. The presented research is a continuation of previously published work about EB strengthening of slabs against punching shear failure by the authors (Akhundzada et.al 2018; Akhundzada et.al 2019).

EXPERIMENTAL PROGRAMME

Test specimens

The proposed research consists of preparing and testing eight slabs with a central column to present an internal two-way spanning slab-column connection. The slabs have dimensions of 1500×1500×120 mm and column head of 150×150×150 mm as shown in Fig 1. All slabs are reinforced with top (tension) reinforcement of 15H8 @100 c/c and bottom (compression) reinforcement of 8H6 @200 c/c. The column head is reinforced with 4H10 L-bars and 3 No. 6 mm links. The slabs with the above parameters were chosen to ensure that punching shear failure occurs within the test slabs. Two slabs serve as control samples and the remaining six slabs are strengthened with CFRP bars.

The tested specimens are prototypes of an actual flat slab, scaled down by a factor of 0.5. The actual slab is 240 mm thick and is supported by a grid of columns at 6x6 m. The slab has hogging reinforcement of H16 @200 c/c. The spacing of the hogging reinforcement is adjusted to ensure the maximum spacing of rebars is within the allowable limits. The tested slabs only represent the junction between the column and the slab where punching shear failure is supposed to occur.

Material properties

Ready-mix concrete was used for the experiment to imitate real-life construction. The concrete was produced by mixing natural (Thames Valley) aggregates and sand in Portland cement with water to cement ratio of 0.6. One batch of concrete was used to cast the slabs. The concrete was then cured for two weeks by covering it with wet hessian sheets and at a temperature of 26°C. The characteristic cylindrical compressive strength and the characteristic tensile strength of the concrete was determined during the testing day (28 days) according to BS EN 12390-13 (BSI, 2013). The compressive cylinder strength f_c was 30 MPa and the tensile strength f_{ctm} was 2.8 MPa with a standard deviation of 0.65 and 0.71 respectively.

The steel reinforcement has a characteristic yield strength of 500 MPa and is designated as grade 500 (BS, 2005).

The CFRP bars used in this experiment had a spirally wound surface to ensure improved bond with the concrete. Fig 2 shows the cross-sectional area of the CFRP bars used in this experiment. The CFRP bars had a tensile strength of 1800-2200 MPa and elastic modulus of 140-150 GPa with a minimum rupture strain of 0.0129. The CFRP bars had a fibre content of 63%. The surfaces of the CFRP bars were treated with epoxy and were additionally threaded to create a spirally wound surface. The values for the mechanical properties of the CFRP bars were provided by the manufacturer and were based on the nominal cross-sectional area. A commercially available two-component (resin and polyamine hardener) structural adhesive was used to bond the CFRP bars to concrete. The structural adhesive (WEBER, 2021) had a compressive strength of 85 MPa and tensile strength of 17 MPa. The elastic modulus for the epoxy adhesive was 9.8 GPa.

Strengthening with CFRP

The grooves at the tension surface of the slab for this research were created by placing timber strips into fresh concrete and were removed after hardening. The use of wooden strips or foam for creating the grooves in concrete is widely used in NSM related research (Novidis et.al 2007;

Wahab et.al 2011; Gopinath et.al 2016). The cross-sectional geometry of the grooves was square, and its dimensions were (*1.5*d_b *x 1.5*d_b) where d_b is the diameter of the CFRP bars. Fig 3 shows the typical groove detail of the 8mm CFRP bar. The groove dimensions fell within the optimum values indicated by Lee et.al (2013). The CFRP bars were cleaned with white spirit and the dust was removed from the grooves to ensure a stronger bond between the CFRP bars and the concrete. The epoxy adhesive was mixed with a paddle mixer and put onto a mortar gun. The grooves were then partially filled with the mortar gun and the CFRP bars were placed and pressed into the grooves. The remaining cavity was filled with epoxy and the surface was flattened with a trowel. The process of preparation and strengthening the slabs is shown in Fig 4.

Strengthening layout

The details of the strengthened samples with NSM CFRP bars as shown in table 1. The CFRP bars are positioned in orthogonal directions by using two strengthening layouts as shown in Fig 5. Four bars are used for strengthening layout one and eight bars are used for strengthening layout two. The bars are positioned at a distance of 60 mm from the perimeter of the column at the tension surface of the slab in the first layout. In the second layout, the bars are positioned around the perimeter of the column and also at a distance of 120 mm from the perimeter to the column. The two strengthening layouts chosen for this research effectively intercepts the punching shear crack and is expected to utilize the maximum capacity of the strengthening material. The chosen layouts will allow for the development of dowel forces in the CFRP reinforcement at the intersection point with the inclined shear crack as indicated in Fig 5. Three different bar diameters are used for each of the strengthening layouts i.e., 6 mm, 8 mm and 10 mm.

Instrumentation and test set up

The response of the slab under monotonic loading was monitored by the instrumentation shown in Fig 6. Five linear variable displacement transducers (LVDTs) were used to measure the vertical displacement of the slab. The LVDTs were positioned at the middle, quarter-span and close to support of the slab. Three strain gauges (SGs) were attached at the mid-point of steel reinforcement to monitor the development of strain in steel reinforcement. Furthermore, four SGs were attached to the mid-point of the CFRP bars and additional six strain gauges were attached to the tension surface of the concrete. Four dial gauges (DGs) were positioned over the supporting frame to measure the movement of the testing rig.

The test set up is shown in Fig 7 and 8. The load was applied through the column head in an upward direction. Eight rectangular hollow sections (RHS) columns were bolted to a strong concrete floor to provide support for the slab. The slab was supported on top and bottom by steel angles bolted to RHS. Smooth surface steel bars were placed between the slab and the angles to allow free rotation of the slab at the edges. The slab was simply supported on four sides. A stress distributor plate was placed under the column to prevent localized crushing of the concrete. A load cell was positioned over the hydraulic jack to monitor the load. The minor deformation of the testing rig was monitored throughout the loading and was taken into consideration during the analysis. The displacement measuring instruments were supported by a light steel frame built above the testing rig and was not connected with the rig. The load application was force-controlled and was applied at a rate of 1 kN/min and the readings were captured at a rate of 0.1 sec.

EXPERIMENTAL RESULTS

Failure modes

All of the tested samples failed under a classical punching shear failure at the point of ultimate load. With the increasing level of load, the initial cracking developed in the radial direction. The punching shear circular crack started to develop away from the perimeter of the column towards the later stages of loading. A sudden drop in the load was observed after reaching the maximum capacity, which is considered as the failure point. The column head with a truncated slab section was physically separated from the slab. In all cases, the failure was abrupt and happened without initial warning signs. The CFRP bars kept a strong bond with the concrete throughout the loading process. The rupture and bond failure of CFRP bars were neither observed nor recorded during the test. A typical failure of one of the strengthened samples is presented in Fig 9.

Load-displacement response

The mid-span deflection of the slab is taken as the difference between the deflection of the slab and the average vertical displacement of the supporting frame. The load-displacement relationship at the centre of the slab for strengthening layouts 1 and 2 are shown in Fig 10. This relationship was linear for all the slabs before the formation of the first crack in the concrete. In radial direction the first crack appeared at a loading level of between 40-50 kN for all samples. At this stage, the slabs displayed a stiff response which could be attributed to the un-cracked concrete section. After the first crack, the load-displacement relationship was majorly dependent on the cross-sectional area of CFRP bars and the strengthening layout.

The first circular crack around the perimeter of the column for control samples CS1 and CS2 started to shape at load of 110-120 kN which caused higher deformability in the load-displacement graph Fig 10. The deformability of the control samples kept increasing as the rate and number of cracks started to increased. The average deflection at the centre of the slab for the samples strengthened with layout one (L1-6, L1-8, L1-10) and layout two (L2-6, L2-8, L2-10) was correspondingly 38% and 41% lower compared to control samples at the point of maximum load. The deformability of the samples strengthened with CFRP bars was lower compared to control samples. Slabs L1-6 and L2-6 exhibited higher deformability amongst the strengthened cases after reaching a load of 135 kN. The larger deformability of these samples could be attributed to small bar diameter allowing for relatively larger deflection throughout the loading.

Flexural stiffness

The flexural stiffness is defined as the ratio between the ultimate load and the maximum deflection at the mid-point of the slab. This ratio explains the deformability of the samples in relation to their ultimate load as indicated in Fig 11. The flexural stiffness is calculated in two stages, before and after the concrete cracking.

In general, the strengthened samples displayed significantly higher stiffness compared to the control samples during the two stages. The difference in the stiffness of the control and strengthened samples are relatively low before the cracking of the concrete. As the concrete starts to crack, the difference increases accordingly. On average, the increase in stiffness for the samples using strengthening layout one and two were 1.76 and 2.75 respectively before the cracking of the concrete. However, this ratio increased to 2.11 and 3.6 for the two strengthening layouts after cracking of the concrete. It could be extrapolated that the degree of dowel action from the CFRP bars contributing towards higher stiffness of the slab is higher after cracking of the concrete.

The increase in stiffness is directly proportional to the increase in cross-sectional area and the number of CFRP bars. The samples with strengthening layout 2 displayed higher stiffness compared to the samples with strengthening layout 1 due to higher number of CFRP bars. The samples with larger diameter of CFRP bars exhibited higher stiffness within their corresponding strengthening layout. Sample L2-10 displayed the highest and sample L1-6 displayed the lowest increase in stiffness compared to the average stiffness of the control samples.

<u>CFRP strains</u>

The load-strain curve at the mid-point of the CFRP bars is shown in Fig 12. The linear behaviour of the load-strain curve at the initial stages of loading shows that the concrete is not cracked. This behaviour changes after initiation of micro-cracking and development of substantial cracks in the tension surface of the slab.

The CFRP and the concrete maintained their bond which did not fail under the increasing monotonic loading during the whole process of testing. This behaviour is well illustrated by the increasing level of strain in relation to the increase in load. The rupture of the CFRP bars was not observed during the test and the slabs failed by the formation of the circular punching shear crack in the concrete. The bars were exposed via removing the epoxy cover after the failure to check for their integrity and it was cross-checked with the data from strain gauges.

The CFRP bars reached up to 45% of its rupture strain before failure of the slab. The strain utilization was relatively higher for samples L1-6 and L2-6. On the other hand, samples L2-8 and L2-10 exhibited the lowest level of strain at any given point of loading amongst all other strengthened samples.

<u>Concrete strain</u>

The concrete strain in the radial direction at the centre, quarter-span, and end of the slabs is shown in Fig 13. The strain readings presented are taken at the peak-load before failure of the slabs. The strain profile along the loading span is similar to a natural distribution curve i.e., it is highest at the centre of the slab and exponentially decreases with the distance along the span. The slabs developed severe cracking at the point of maximum load reaching strains of 0.02.

Eurocode 2 (EC2 2004) requires checking the shear resistance at the face of the column and at the basic control perimeter of *2d* (where *d* is the effective depth of the slab) from the face of the column. The critical section of 2d is shown in dotted line in Fig 15. The capacity of the slab should exceed the applied shear forces at these critical perimeters. The stress concentration is significantly lower outside these perimeters. This shows that the maximum concentration of stresses are within basic the control perimeters and the punching shear failure plane is likely to form inside this region, for slabs without shear reinforcement.

<u>Cracking</u>

When the slabs were subjected to vertical load, the first cracks were formed in the radial direction at the tension surface of the slabs. A circular crack around the perimeter of the column started to develop at a load level of 70-100 kN as shown in Fig 14. The radial cracks kept increasing in the circumferential direction. The punching shear crack started to develop after a significant increase in load away from the face of the column. The failure occurred by full physical separation of a truncated conical surface from the remaining parts of the slab. The cracking was detected by visual observation and recorded throughout the testing.

The first crack for both control samples CS1 and CS2 appeared at a load of around 41 kN and formed at random locations on the tension surface of the slabs. The formation of the first crack for samples with strengthening layout one L1-6, L1-8 and L1-10 occurred on average at a load of 45 kN. The samples with strengthening layout two L2-6, L2-8 and L2-10 delayed the appearance of the first crack and it was formed at a load of around 48 kN. The position and length of the first cracks for the CFRP strengthened samples were in orthogonal direction, parallel to the CFRP strips. The crack formed as a straight line in the middle of the slab, going from one end to the other end and crossing over the column-head. However, the first crack formed at random locations in the radial direction for control samples CS1 and CS2.

The punching shear crack was roughly circular and appeared at some distance away from the vicinity of the column. Strengthening the slabs with NSM CFRP bars did not change the shape of punching shear crack. The shear failure plane developed partially at random locations at the tension surface of the slab and kept growing until failure. The formation of cracks in the epoxy adhesive (used to attach NSM bars to concrete) occurred at later stages of loading compared to concrete. This could be attributed to the higher flexural capacity of the epoxy.

Ultimate punching shear capacity

The maximum capacity of the tested samples is presented in Table 2. The control samples CS1 and CS2 failed under classical punching failure after reaching a maximum load of 141 kN and 146 kN respectively. The retrofitted samples with CFRP bars displayed significantly higher punching capacity compared to the average failure load of the two control samples. The capacity of the strengthened samples within each of the strengthening layout was very similar. Increasing the cross-sectional area of the CFRP bars did not have any noticeable influence on the ultimate capacity in this case. The maximum strain recorded for CFRP bars was around 45% of its rupture strain (refer to Fig 12). The maximum allowable capacity of the CFRP bars was not utilized and the samples failed under concrete shear failure.

Increasing the number of CFRP bars considerably improved the ultimate load. The samples with strengthening layout one (L1-6, L1-8 and L1-10) increased the ultimate load by about 18%. The average increase for strengthening layout two (L2-6, L2-8 and L2-10) was around 41% compared to control samples. Sample L2-10 exhibited the highest increase amongst other strengthened cases and increased the ultimate load by 44%. Positioning the CFRP bars over a larger area intersected the punching shear failure plane at several locations and delayed the punching shear failure, which subsequently translated into enhanced load-carrying capacity.

ANALYTICAL PREDICTIONS

Design codes expressions

The existing design codes predict the punching shear capacity of conventional steel-reinforced concrete only. The ultimate load is obtained by considering several factors such as steel reinforcement ratio, compressive strength of concrete, slab depth and size of the column. The design guidance requires checking the punching capacity of slabs at the face of the column and at critical perimeters. The FIB Model Code (FIB MC, 2010) defines the critical perimeter at a distance of *0.5d* (where *d* is the depth of slab) from the face of the column. The Eurocode 2 (EC2, 2004) identifies the critical perimeter at *2d*. Fig 15 shows the location of critical/control perimeter according to the design codes. The following expressions, without considering capacity reduction factors, are adopted for estimating the punching capacity of slabs without shear reinforcement. The following expressions are used for the purpose of comparison with the design codes.

Eurocode 2

Eurocode 2 (EC2, 2004) proposes the following expression to estimate the punching shear capacity of RC slabs.

$$V_c = 0.18k(100\rho_1 \cdot f_{ck})^{1/3} \cdot d \cdot u + k_1\sigma_{cp} \geq \left(V_{min} + k_1\sigma_{cp}\right) \quad (1)$$

$$k = 1 + \sqrt{{}^{200}/_{d}} \leq 2 \quad (2)$$

$$\rho = \sqrt{(\rho_{1z} \cdot \rho_{1y)}} \leq 0.02 \quad (3)$$

$$V_{min} = 0.035k^{3/2}{f_{ck}}^{1/2} \quad (4)$$

In the above expressions, d represents the effective depth of the slab, u represents the critical control perimeter, term k is a size factor, ρ_1 is the flexural reinforcement ratio, f_{ck} is the characteristic compressive strength of concrete, σ_{cp} is a factor related to prestressing and V_{min} shows the minimum shear capacity.

FIB MC 2010

FIB MC (2010) provides four levels of approximation denoted by term ψ for calculating the rotation of the slab. The level one approximation is used in this instance due to negligible redistribution of moments.

$$V_{rc} = k_{\psi} \times f_{ck} \times u \times d \quad (5)$$

$$k_{\psi} = \frac{1}{1.5 + 0.9k_{dg}\psi d} \leq 0.6 \quad (6)$$

$$k_{dg} = \frac{32}{16 + d_g} \quad (7)$$

$$\psi = 1.5 \times \frac{r_s}{d}\frac{f_{yd}}{E_s} \quad (8)$$

The term k_ψ is related to the rotation of the slab, d_g is the maximum size of aggregate used in concrete, r_s is the radius of the separated slab element, f_{yd} is the yield strength of steel and E_s is the elastic modulus of flexural reinforcement.

<u>Adoption of Chen & Li method for NSM</u>

The design codes previously discussed estimate the punching capacity of slabs at critical perimeters by considering effective depth, reinforcement ratio and compressive strength of the concrete. However, there are no known design codes for calculating the punching capacities of slabs strengthened with NSM CFRP bars. The design approach adopted in this study is based on Chen & Li (2005) method. This design approach considers FRP as flexural reinforcement and introduces two terms to be replaced in the design codes. The term ρ_{eqv} and d_{eqv} are introduced to replace ρ and d to take the influence of reinforcement ratio and effective depth into consideration.

This method assumes a perfect bond between the concrete and the CFRP bars. This assumption is true for this experiment and it was confirmed by visual inspection and strain data. The distribution of forces, stresses, and strains within the cross-section of the slab is presented in Fig 16. It should be noted that the diagram is modified to change the EBR FRP to NSM FRP strengthening. According to this approach, the maximum flexural capacity is achieved, when the concrete reaches strain of 0.003 or the CFRP reaches its rupture strain. The strain in CFRP bars and steel reinforcement is determined by linear strain distribution.

$$\varepsilon_s = \frac{d-c}{c}\varepsilon_{cu} \qquad (9)$$

$$\varepsilon_f = \frac{h_1-c}{c}\varepsilon_{cu} \qquad (10)$$

In the expressions above, ε_s is the strain in steel reinforcement; ε_{cu} is the strain in concrete which is taken as 0.003 and ε_f is the strain in CFRP bars. The stresses in steel and CFRP bars can be found using the following expressions:

$$f_s = E_s \varepsilon_s \text{ for } \varepsilon_s < \varepsilon_y \quad (11)$$

$$f_s = f_y \text{ for } \varepsilon_s \geq \varepsilon_y \quad (12)$$

$$f_f = E_f \varepsilon_f \text{ for } \varepsilon_f < \varepsilon_{fu} \quad (13)$$

Where ε_y and ε_{fu} shows the yield and ultimate strain in CFRP bars; f_y is the yield stress of flexural steel reinforcement; E_f is the CFRP elastic modulus and E_s is the steel elastic modulus.

The compression force in concrete, tension force in steel reinforcement and tension force in CFRP bars is obtained from the following expressions:

$$C_c = 0.85 f'_c ab \quad (14)$$

$$T_s = A_s f_s \quad (15)$$

$$T_f = A_f f_f \quad (16)$$

In the expressions above, a is the depth of rectangular stress block; b is the unit width of the slab and the cross-sectional area of steel reinforcement and the CFRP bars is denoted by A_s and A_f.

The depth of the neutral axis is obtained by conducting iterations of the equilibrium of internal forces until the following equation is satisfied.

$$C_c = T_s + T_f \quad (17)$$

After taking moment about the steel reinforcement axis, the following expression is obtained:

$$M_{nf} = C_c\left(d - \frac{a}{2}\right) + T_f(h_1 - d) \quad (18)$$

The influence of the CFRP bars and their positioning with respect to the depth of the slab could be calculated backwardly.

$$d_{eqv} = \frac{M_{nf}}{T_s + T_f} + \frac{a}{2} \qquad (19)$$

$$\rho_{eqv} = \frac{T_s + T_f}{b d_{eqv} f_s} \qquad (20)$$

The terms d_{eqv} and ρ_{eqv} are then substituted in the design codes to obtain the ultimate capacity of strengthened slabs.

Comparison of results

The ultimate capacities obtained from the experimental work and the capacities from the design codes are presented in table 2. The predictions of both Eurocode 2 (2014) and FIB MC (2010) are somewhat similar for estimating the punching capacities of the two control slabs CS1 and CS2. However, the predictions of the modified design codes were relatively conservative for the strengthened slabs using Chen & Li's (2005) method. In general, these predictions provided more accurate values for the samples strengthened with layout one as compared to samples strengthened with layout two.

Chen and Li's method restricts the concrete strain to 0.003 but during the experiment, a significantly higher level of strain was recorded at the centre of slabs (refer to Fig 12). The model also assumed full bond of CFRP with concrete which was observed during the experiment for all slabs. This method could be used for estimating the punching capacitates of flat slabs strengthened with NSM FRP bars.

DISCUSSION

According to Moe (1961), the punching shear strength of flat slabs can be established from its flexural capacity. Increasing the flexural reinforcement of flat slabs directly improves its flexural capacity, but it also indirectly contributes to the punching shear capacity. Therefore, the provision of flexural NSM CFRP reinforcement enhances the punching shear capacity of flat slabs. This effect is more pronounced for slabs with lower reinforcement ratio. The NSM reinforcement around the perimeter of the column intersects the punching shear crack and delays its growth. Introducing greater numbers of CFRP bars around the punching area is more effective as it increases the number of intersection points with the shear crack.

Changing the cross-sectional area did not noticeably influence the ultimate load because the CFRP bars did not reach their rupture strain. The slabs were over-strengthened in this specific case. A relationship between the cross-sectional area of the CFRP bars and the ultimate capacity could be established if the failure occurs via rupture of the CFRP bars. This relationship can be achieved by using smaller CFRP bar sizes.

The increase in the ultimate load for the strengthened samples is due to the development of dowel forces in the CFRP bars when they cut across the inclined shear crack. When the conically shaped crack is developed over the column head, it creates a shear failure plane with the remaining parts of the slab. These shear forces are resisted by the aggregate interlock and dowel action of the steel and CFRP reinforcement. The CFRP reinforcement restricts the crack widening by the development of dowel forces. The concrete cover is the main parameter upon which the dowel mechanism is dependent (CEB-FIP 1993; CEB 1996). Deeper concrete cover and higher tensile splitting strength of concrete allow for the development of higher level of dowel forces. The samples strengthened with layout two developed twice the amount of dowel forces compared to samples strengthened with layout one, due to the amount of CFRP bars. Fig 17 shows the variation in the dowel forces between the two strengthening schemes.

The development of vertical forces due to the membrane effect in the CFRP reinforcement is also contributing towards increasing the ultimate load. Kinnunen and Nylander (1960) examined the contributions from the dowel forces and the membrane effects, for the punching shear capacity of flat slabs. According to their conclusion, slab punching shear capacity improves if the ratio and strength of flexural reinforcement increases.

Sample L1-8 and L2-6 were strengthened with roughly the same amount of CFRP reinforcement but the increase in the ultimate load for sample L2-6 was two times greater than sample L1-8. Sample L2-6 satisfied the maximum bar spacing in the area affected by punching shear whilst sample L1-8 had large unreinforced regions, which allowed for the development of punching shear crack at a relatively lower level of loading.

Alexander and Simmonds (1990) concluded that the concentration of reinforcement over the column strip is less effective compared to equal distribution of reinforcement over a wider area. The equal distribution of reinforcement allowed for further development of dowel forces, which subsequently delayed the punching shear failure.

Strengthening slab-column connections with NSM CFRP bars significantly increases the cracking load, stiffness, and ultimate capacity. The bonded length provided for the CFRP bars is sufficient for this specific size of the slab. The CFRP bars forms a strong bond with concrete and the system does not suffer from debonding. This results in utilizing the maximum allowable capacity of CFRP bars which subsequently enhances the ultimate load. The NSM strengthening of slab-column connection is significantly more efficient than EBR strengthening mainly in terms of bond performance and increasing the ultimate load.

The negative moment (hogging) region in flat slabs specifically in car parks is exposed to heavy vehicular impact. External strengthening with FRP EBR causes durability issues and poses a major fire risk. The use of NSM as an alternative to EBR strengthening overcomes such issues. It should be noted, that the NSM method requires sufficient concrete cover for creating grooves in concrete.

CONCLUSIONS

In this study, the punching shear strength of interior slab-column connections retrofitted with NSM CFRP bars is experimentally investigated. The study concentrates on the influence of the cross-sectional area of CFRP bars and the strengthening layout. Eight slab-column connections were tested under monotonic load and the following conclusions are drawn:

1. The use of NSM CFRP bars improves the shear capacity of slab-column connections. Sample L2-10 increased the ultimate load by up to 44% compared to control samples.
2. Increasing the number of CFRP bars considerably enhances their ultimate load. The average strength gain for strengthening layout one and two is 18% and 41% respectively.
3. Strengthening delays formation of the first crack in concrete which subsequently results in maintaining a linear relationship for load-displacement and load-strain curves.
4. CFRP NSM strengthening significantly increases the flexural stiffness. The increase in stiffness is directly related to the strengthening layout and the cross-sectional area of CFRP bars. The maximum flexural stiffness was recorded for sample L2-10 which shows an increase of 100% compared to control samples.
5. The ultimate capacities of strengthened slabs with NSM CFRP bars can accurately be calculated by the adoption of Chen & Li's method in the design codes. The proposed method could be incorporated into design codes.

NOTATION

A_f	Cross-sectional area of FRP reinforcement
A_s	Cross-sectional area of steel reinforcement
a	Depth of the rectangular stress block
b	Breadth of the slab
C_c	Compression force in the concrete
c	Column side length (dimension)
d	Effective depth of the slab
d'	Height of concrete cover
d_b	Diameter of the bar
d_{eqv}	Equivalent effective depth for the slab
d_g	Maximum aggregate size in concrete mix
d_g	Concrete cover on the side of the slab
E_f	Modulus of elasticity for FRP
E_s	The modulus of elasticity for steel
f_{ck}	Compressive strength of concrete
f'_c	Compressive strength of concrete
f_y	Yield strength of steel
h	Depth of the slab section

h_1	Height between the compression surface of the concrete to the centre of the FRP reinforcement in the slab
k	Size factor for the effective depth of the slab
k_1	Empirical factor representing the nominal stresses
k_{dg}	Parameter related to the maximum aggregate size
k_{ψ}	Parameter related to the rotation of the slab
T_f	Tensile force in the FRP reinforcement
T_s	Tensile force in the steel reinforcement
u	Length of the control perimeter in the slab
u_0	First perimeter of the column
V_{min}	Minimum shear capacity of the slab
$V_{u,predicted}$	Maximum punching shear capacity predicted by the design codes
$V_{u,test}$	Maximum punching shear capacity of the tested samples
γ_s	Radius of the separated slab element
ε_{cu}	Strain in the concrete
ε_f	Strain in the FRP reinforcement
ε_{fu}	Ultimate strain in the FRP
ε_s	Strain in the steel reinforcement
ε_y	Yield strain in the FRP
π	Ratio of circle circumference to its diameter (constant)

ρ	Flexural steel reinforcement ratio
ρ_1	Average reinforcement ratio
ρ_{1y}	Reinforcement ratio in Y-Y direction
ρ_{1z}	Reinforcement ratio in Z-Z direction
ρ_{eqv}	Equivalent reinforcement ratio for the slab
σ_{cp}	Concrete stresses due to prestressing of reinforcement
Ψ	Angle between the horizontal axis and the deformed slab

DATA AVAILABILITY STATEMENT

Some or all data, models, or code that support the findings of this study are available from the corresponding author upon reasonable request. The data includes:

1. Pictures showing the failure mode of all samples
2. Deflection of the samples at quarter-span
3. Strain development in steel reinforcement
4. Excel sheets showing the detailed calculation for obtaining the analytical results

REFERENCES

Abdul-Kareem, A.H. 2019. “Punching Strengthening of Concrete Slab-column Connections Using Near Surface Mounted (NSM) Carbon Fiber Reinforced Polymer (CFRP) Bars.” *Journal of Engineering Research and Reports.,* 9(2), 1-14.

Abdullah, A. Bailey, CG. Wu ZJ. 2013. “Tests investigating the punching shear of a column-slab connection strengthened with non-prestressed or prestressed FRP plates.” *Construction and Building Materials.,* 48, 1134-1144.

Agbossou, A. Micheal, L. Lagache, M. and Hamelin, P. 2008. “Strengthening slabs using externally-bonded strip composites. Analysis of concrete covers on the strengthening.” *Composites: Part B.,* 39 (1), 1125-1135.

Akhundzada, H. Donchev, T. Petkova, D. and Samsoor, A.B. 2018. Influence of the positioning of CFRP laminates for improving punching shear capacity of column-to-slab connections. *ACI Special Publication*., (SP 327): 18.1-18.8.

Akhundzada, H. Donchev, T. and Petkova, D. 2019. “Strengthening of slab-column connection against punching shear failure with CFRP laminates.” *Composite Structures.,* 208 (1), 656-664. https://doi.org/10.1016/j.compstruct.2018.09.076

Alexander, S.D.B. and Simmonds S.H. 1992. “Tests of column-flat plate connections.” *ACI Structural Journal.,* 89(5), 495-502.

Azizi, R. Talaeitaba, S. 2019. “Punching shear strengthening of flat slabs with CFRP on grooves (EBROG) and external rebars sticking in grooves.” *International Journal of Advanced Structural Engineering.,* 11, 79-95.

Bilotta, A. Ceroni, F. Nigro, E. and Pecc, M. 2015. “Efficiency of CFRP NSM strips and EBR plates for flexural strengthening of RC beams and loading pattern influence.” *Composite Structures.,* 124 (1), 163-175.

Binici, B. Bayrak, O. 2005. “Use of fiber-reinforced polymers in slab-column connection upgrades.” *ACI Structural Journal.,* 102, 93-102.

BSI (British Standards Institution). 2013. *Testing hardened concrete. Determination of secant modulus of elasticity in compression*. BS EN 12390-13. London, United Kingdom. https://doi.org/10.3403/BSEN12390

BS (British Standards). 2005. *Steel for the reinforcement of concrete. Weldable reinforcing steel. Bar, coil and decoiled product. Specification.* British Standard Association. BS 4449:2005+A3:2016

CEB-FIP (Comite European Du Beton – Federation International Du Precontrainte). 1993. *Model Code* 1990.

CEB- (Comite European Du Beton). 1996. *RC elements under cyclic loading.*

Chen, C.C. and Li, C.Y. 2005. “Punching shear strength of reinforced concrete slabs strengthened with glass fiber-reinforced polymer laminates.” *ACI Structural Journal*., 102 (4), 535-542.

De Lorenzis, L. and Teng, J.G. 2007 “Near-surface mounted FRP reinforcement: an emerging technique for strengthening structures.” *Composites: Part B*., 38 (1), 119–43.

Elbakry, H.M.F. and Allam, S.M. 2015. “Punching strengthening of two-way slabs using external steel plates.” *Alexandria Engineering Journal.,* 54 (1), 1207-1218.

El-Salakawy, EF. Polak, MA. and Soudki, KA. 2004. “New shear strengthening technique for concrete slab-column connections.” *ACI Structural Journal.,* 100(3), 297-304.

Erdogan, H. Binici, B. Ozcebe, G. 2010. “Punching shear strengthening of flat-slabs with CFRP dowels.” *Magazine of Concrete Research.,* 62(7), 465-478.

Esfahani, M.R. Kianoush, M.R. and Moradi, A.R. 2009. “Punching shear strength of interior slab–column connections strengthened with carbon fiber reinforced polymer sheets.” *Engineering Structures*., 31 (1), 1535-1542.

ECS (European Committee for Standardaization) Eurocode 2. 2004. *Design of concrete structures – part 1 – 1: General rules and rules for buildings.*

Farghaly, A. Ueda, T. 2019. “Analytical evaluation of punching strength of two-way slabs strengthened externally with FRP sheets.” *Proceedings of FRPRCS-9 Conference*, Sydney, Australia.

FIB (Federation internationale du beton. Fib model code for concrete structures) 2010. *FIB model code*. Lausanne, Switzerland.

George, J.P. Mohan, R.T. 2020. “Punching Shear Strengthening of Flat Slabs with External Bonded CFRP on Grooves (EBROG).” *Proceedings of SECON 2020.,* 909-915. https://doi.org/10.1007/978-3-030-55115-5_81

Gopinath, S. Murthy, A.R. and Patrawala, H. 2016. “Near surface mounted strengthening of RC beams using basalt fiber reinforced polymer bars.” *Construction and Building Materials.,* 111 (1), 1-8.

Harajli, M. and Soudki, K.A. 2003. “Shear Strengthening of Interior Slab–Column Connections Using Carbon Fiber-Reinforced Polymer Sheets.” *Journal of Composites for Construction.,* 7 (2), 145-153.

Hassan, T. and Rizkalla, S. 2014. “Bond mechanism of near-surface-mounted fiber-reinforced polymer bars for flexural strengthening of concrete structures.” *ACI Structural Journal.,* 101 (6), 830-9.

Kim, YJ. Longworth, JM. Wight, RG. Green, MF. 2010. “Punching shear of two-way slabs retrofitted with prestressed or non-prestressed CFRP sheets.” *Journal of Reinforced Plastics and Composites.*, 29(8), 1206-1223.

Kinnunen, S. and Nylander H. 1960. “Punching strength of reinforced concrete slabs with shear reinforcement, Transactions, No. 158.” *Royal Institute of Technology*: Stockholm, Sweden.

Koppitz, R. Kenel, A. Keller, T. 2014. “Punching shear strengthening of flat slabs using prestressed carbon fiber-reinforced polymer straps.” *Engineering Structures.,* 76, 283-294.

Lawler, N. Polak, MA. 2011. “Development of FRP shear bolts for punching shear retrofit of reinforced concrete slabs.” *Journal of Composites for Construction.,* 15(4), 591-601. DOI: 10.1061/(ASCE)CC.1943-5614.0000188.

Lee, D. and Chang, L. 2013. “Bond of NSM systems in concrete strengthening – Examining design issues of strength, groove detailing and bond-dependent coefficient.” *Construction and Building Materials*., 47 (1), 1512-1522.

Meisami, MH. Mostofinejad, D. 2013. “Nakamura H. Punching shear strengthening of two-way flat slabs using CFRP rods.” *Composite Structures*., 99, 112-122.

Moe, J. 1961. “Shearing strength of reinforced concrete slabs and footings under concentrated loads, in Development Department Bulletin No. D47.” *Portland Cement Association,* Skokie. 130.

Novidis, D. Pantazopoulou, S. and Tentolouris. E. 2007. “Experimental study of bond of NSM-FRP reinforcement.” *Construction and Building Materials*., 21 (8), 1760-70.

Ruiz, M.F. Muttoni, A. and Kunz, J. 2011. “Strengthening of Flat Slabs Against Punching Shear Using Post-Installed Shear Reinforcement.” *ACI Structural Journal*., 107 (4), 434-442.

Seo, S.Y. Feo, L. and Hui, D. 2013. "Bond strength of near surface-mounted FRP plate for retrofit of concrete structures." *Composite Structures*., 95 (1), 719-727. http://dx.doi.org/10.1016/j.compstruct.2012.08.038

Wahab, N. Soudki, K.A. and Topper. T. 2011. "Mechanism of Bond Behavior of Concrete Beams Strengthened with Near-Surface-Mounted CFRP Rods." *Journal of Composites for Construction*., 15 (1), 85-92.

Weber Saint-Gobain (Weber). 2021. Moisture-tolerant epoxy adhesive for structural bonding application. https://www.uk.weber/files/gb/202009/02.020A%20webertec%20EP%20structural%20adhesive.pdf

TABLES

Table 1. Sample description

Slab ID	Strengthening Layout	Number of bars N_b	Bar diameter d_b (mm)	Test variable
CS1	-	-	-	Control slab
CS2	-	-	-	Control slab
L1-6	Layout 1	4	6	Strengthened
L1-8	Layout 1	4	8	Strengthened
L1-10	Layout 1	4	10	Strengthened
L2-6	Layout 2	8	6	Strengthened
L2-8	Layout 2	8	8	Strengthened
L2-10	Layout 2	8	10	Strengthened

Table 2. Comparison of ultimate loads with design codes

Specimen designation	***$V_{u,\ test}$ (kN)***	***$V_{u,\ predicted}$ (kN)***		***$V_{u,\ test}$/ $V_{u,\ predicted}$***	
		EC 2	FIB MC	EC 2	FIB MC
CS1	141	135	128	1.05	1.1
CS2	146	135	128	1.08	1.14
L1-6	168	153	144	1.1	1.17
L1-8	172	161	148	1.07	1.17
L1-10	167	168	150	0.99	1.11
L2-6	202	163	149	1.24	1.36
L2-8	197	174	153	1.14	1.29
L2-10	206	182	155	1.13	1.33
			Average	1.1	1.21

LIST OF FIGURES

Fig. 1. Typical cross-section of the slab (dimensions in mm)

Fig. 2. Cross-sectional area of the CFRP bars (mm)

Fig. 3. Typical groove detail for 8mm CFRP bar (dimensions in mm)

Fig. 4. (a) Steel reinforcement in moulds (b) Finished grooves for strengthening (c) CFRP bars (d) Placing CFRP bars in grooves

Fig. 5. (a) Cross-section layout 1 (b) plan layout 1 (c) cross-section layout 2 (d) plan layout (dimensions in mm)

Fig. 6. Slab instrumentation (dimensions in mm)

Fig. 7. Test set up and instrumentation side view

Fig. 8. Test set up

Fig. 9. Punching failure of slab L2-8

Fig. 10. Load-deflection response at mid-span

Fig. 11. Flexural stiffness of all samples

Fig. 12. Load-strain relationship in CFRP bars

Fig. 13. Strain profile in the tension surface of slabs at ultimate load

Fig. 14. Cracking pattern for control and CFRP strengthened samples

Fig. 15. Critical/control punching shear perimeter for design codes

Fig. 16. Strain, stress and force distribution in slab section

Fig. 17. Development of dowel forces in the strengthened slabs

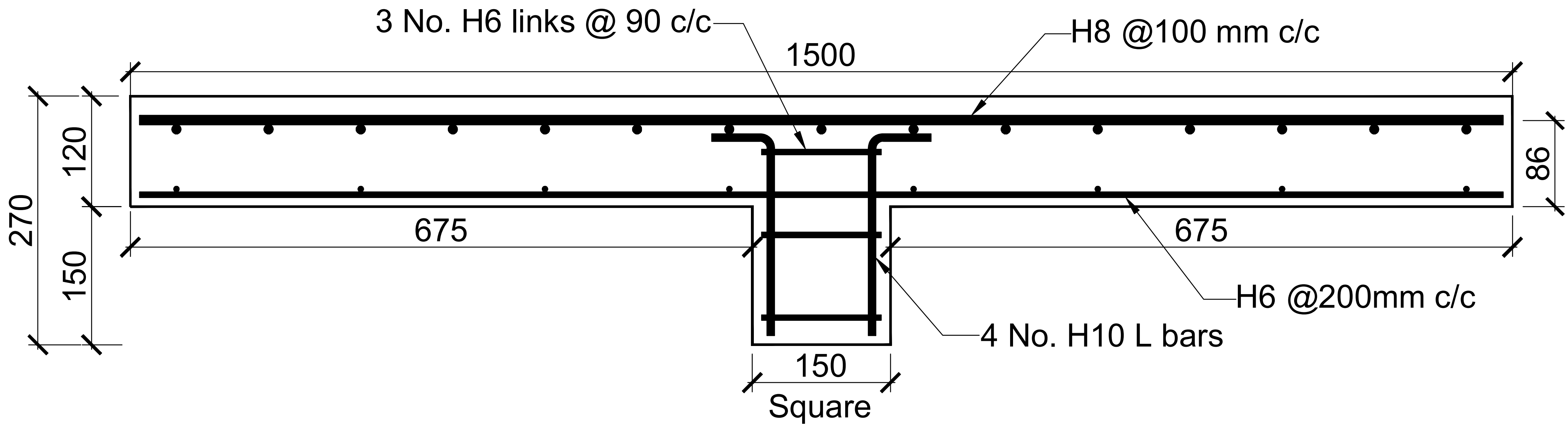
3 No. H6 links @ 90 c/c
H8 @100 mm c/c
1500
98
120
270
150
675
675
H6 @200mm c/c
4 No. H10 L bars
150
Square

Figure 2

Figure 3

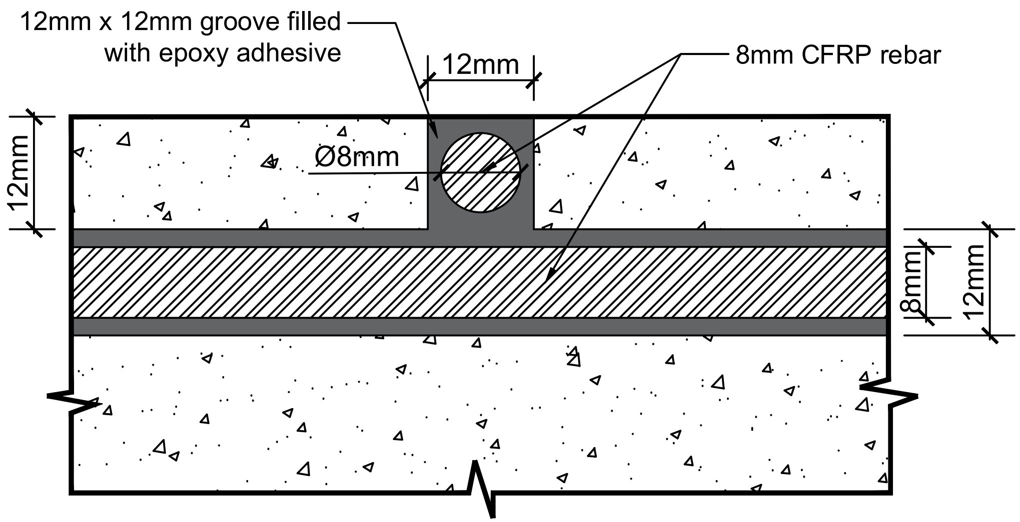
12mm x 12mm groove filled
with epoxy adhesive
12mm
8mm CFRP rebar
Ø8mm
12mm
8mm
12mm

Figure 4

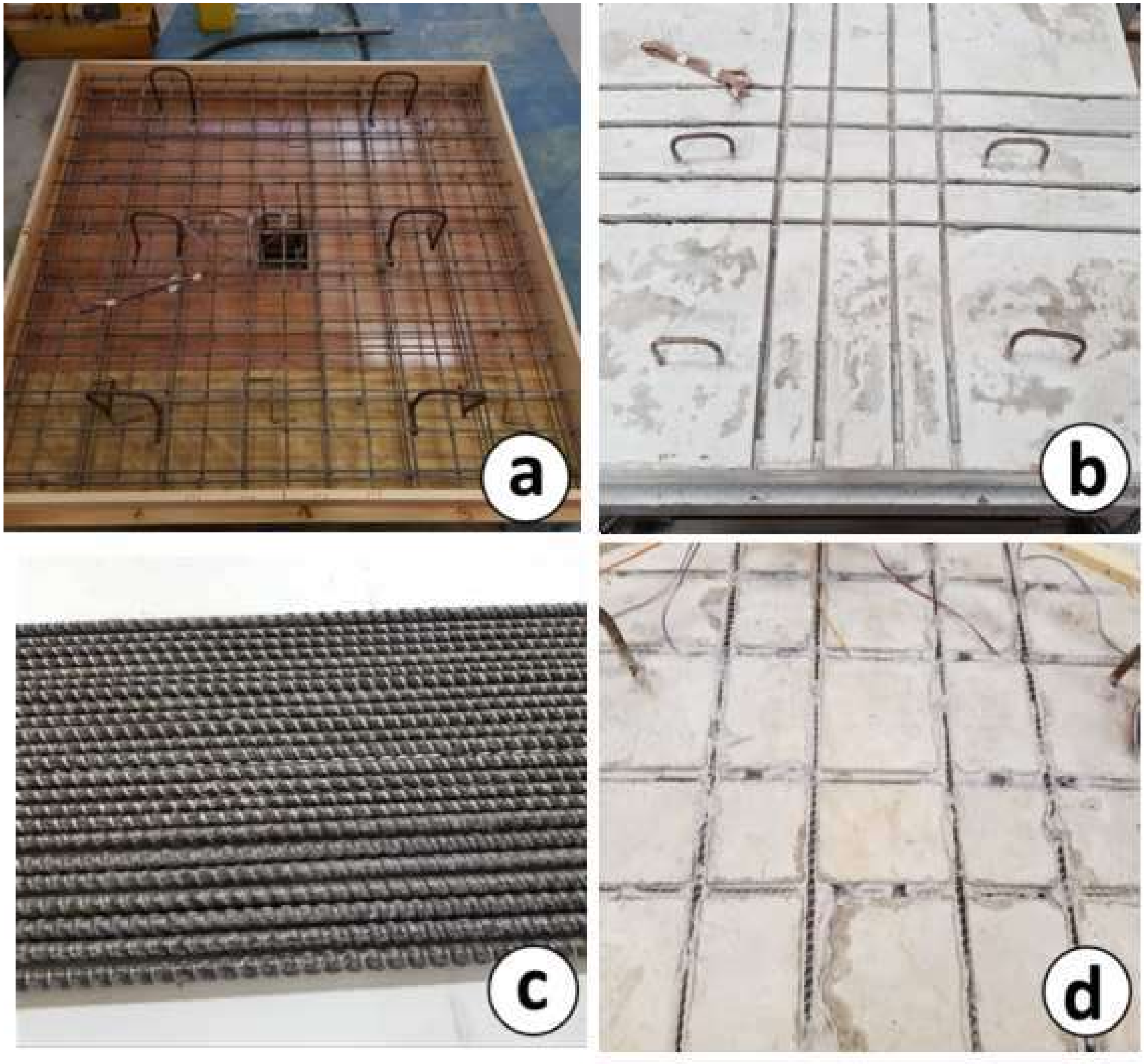

Figure 5

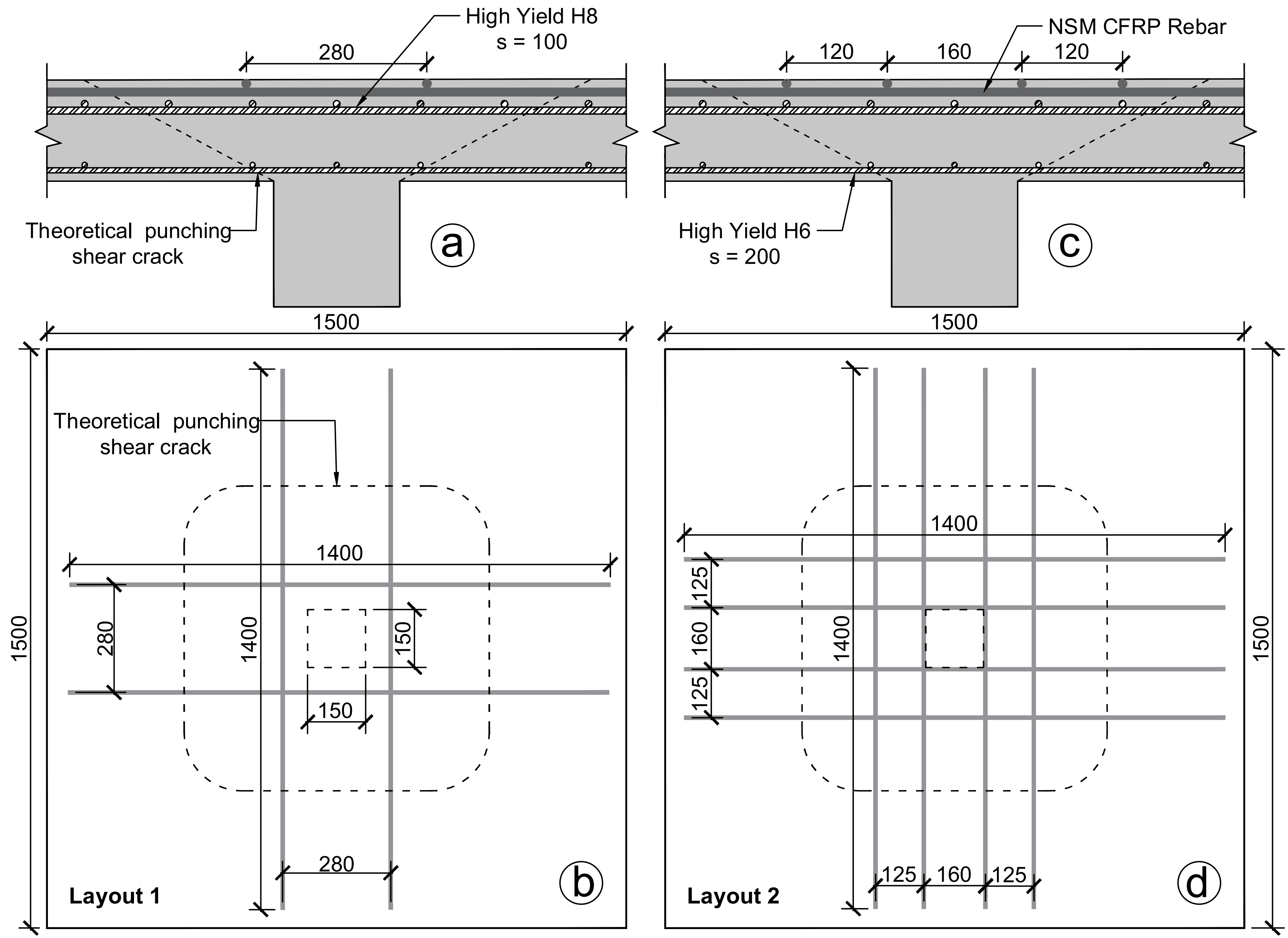

Note: All units are in mm.

Figure 6

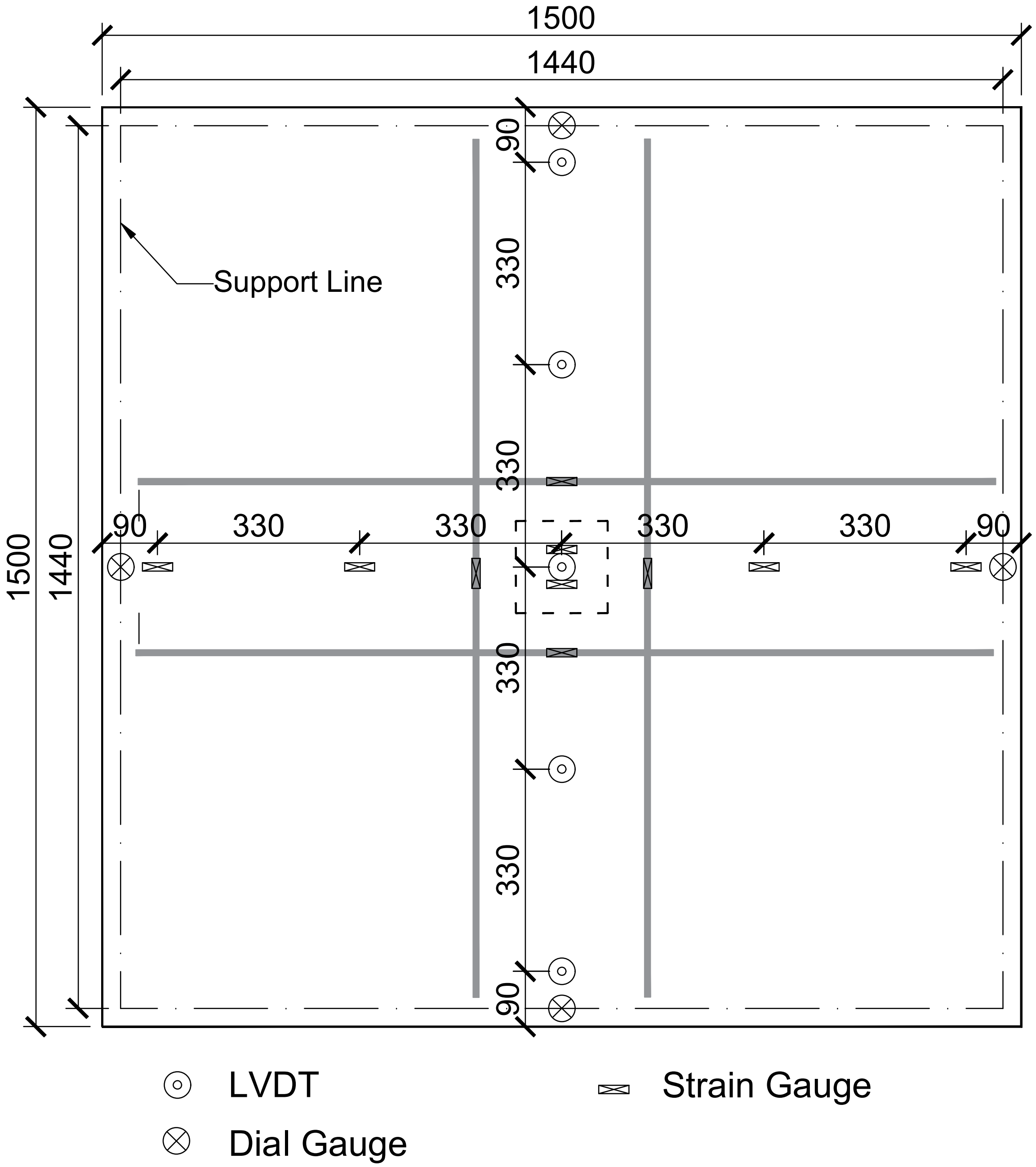
1500
1440
Support Line
90
330
330
330
330
90
1500
1440
LVDT
Dial Gauge
Strain Gauge

Figure 7

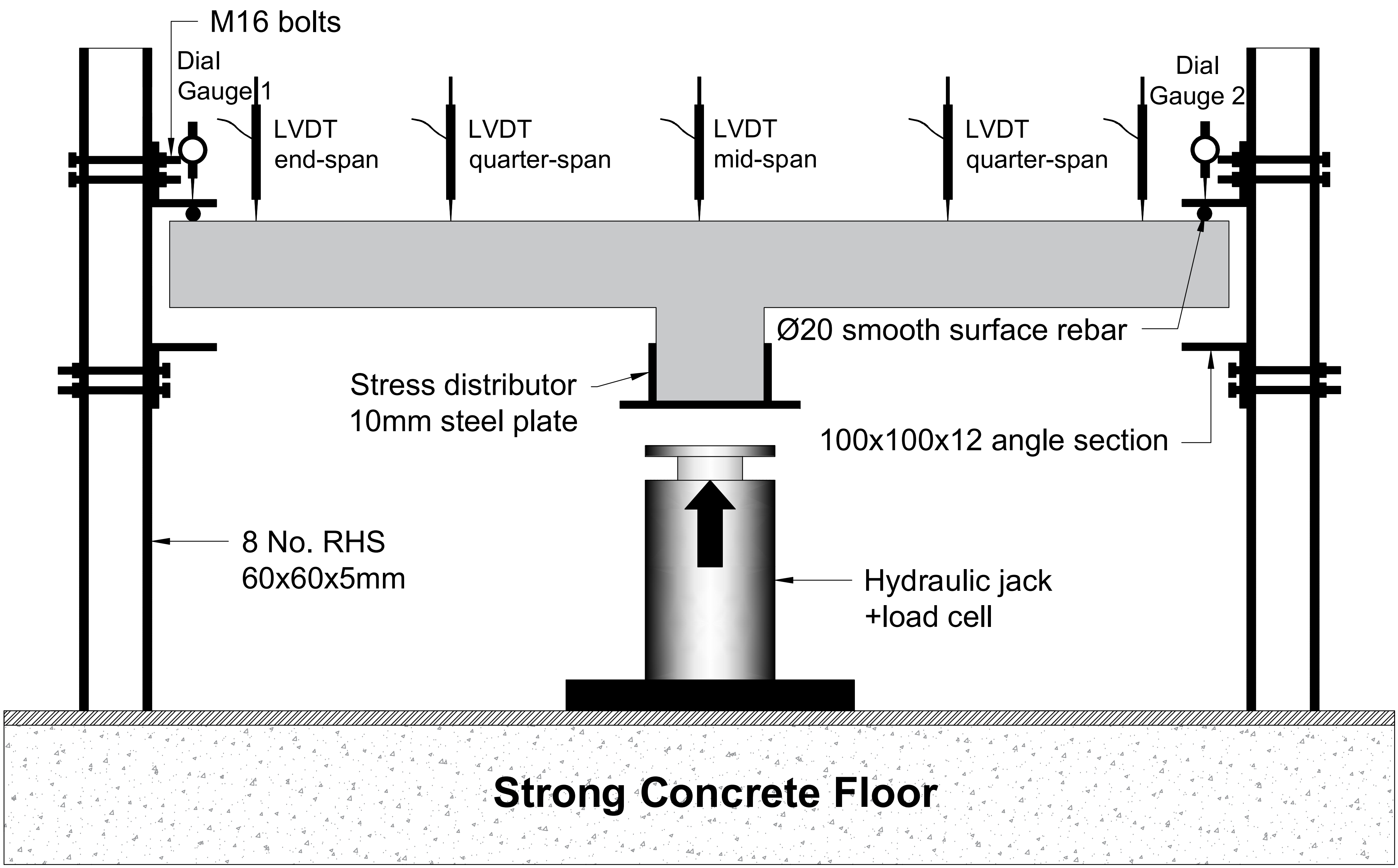
M16 bolts
Dial
Gauge 1
LVDT
end-span
LVDT
quarter-span
LVDT
mid-span
LVDT
quarter-span
Dial
Gauge 2
Ø20 smooth surface rebar
Stress distributor
10mm steel plate
100x100x12 angle section
8 No. RHS
60x60x5mm
Hydraulic jack
+load cell
Strong Concrete Floor

Figure 8

Figure 9

Figure 10

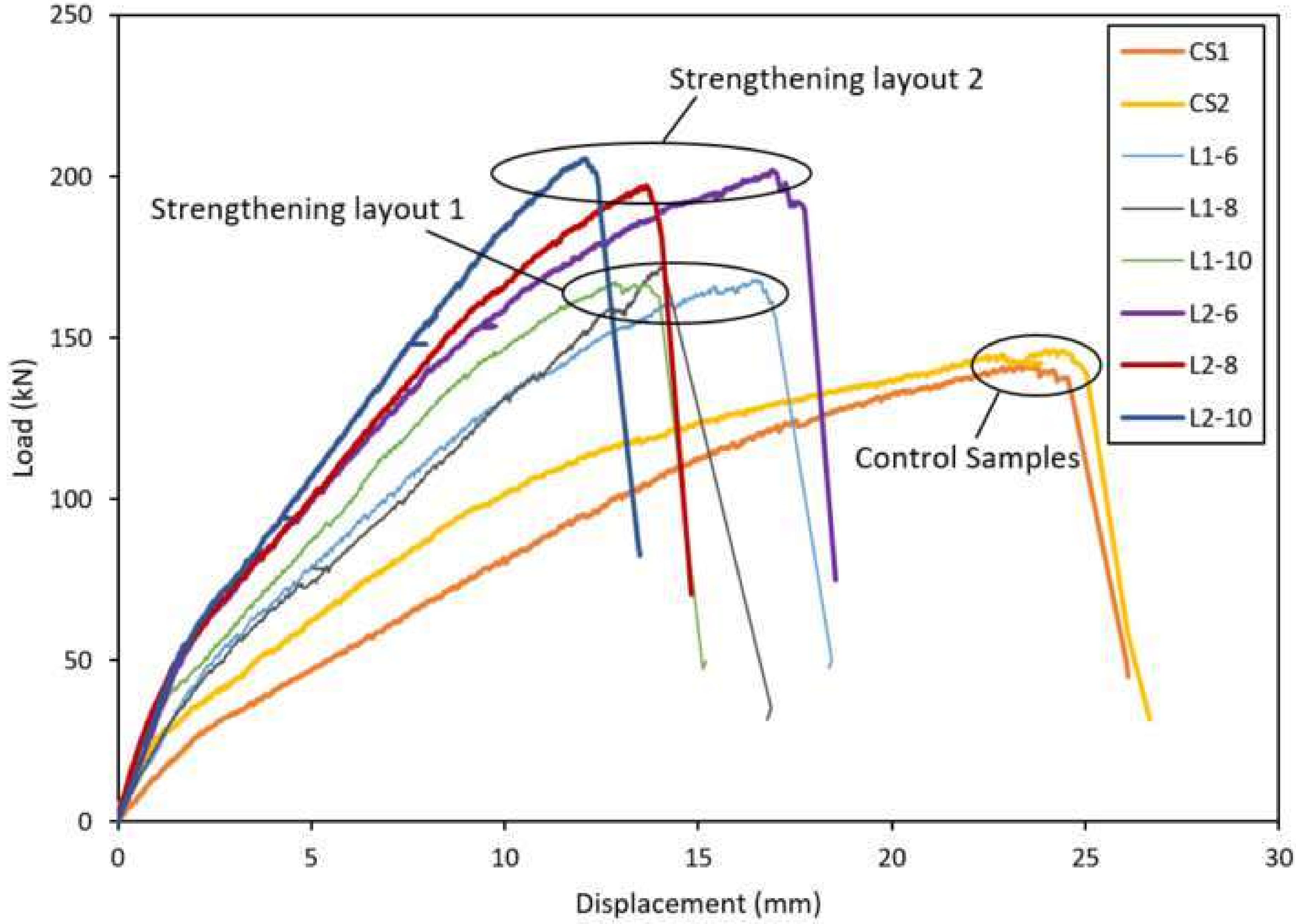
250
200
150
100
50
0
Load (kN)
0
5
10
15
20
25
30
Displacement (mm)
Strengthening layout 2
Strengthening layout 1
Control Samples
CS1
CS2
L1-6
L1-8
L1-10
L2-6
L2-8
L2-10

Figure 11

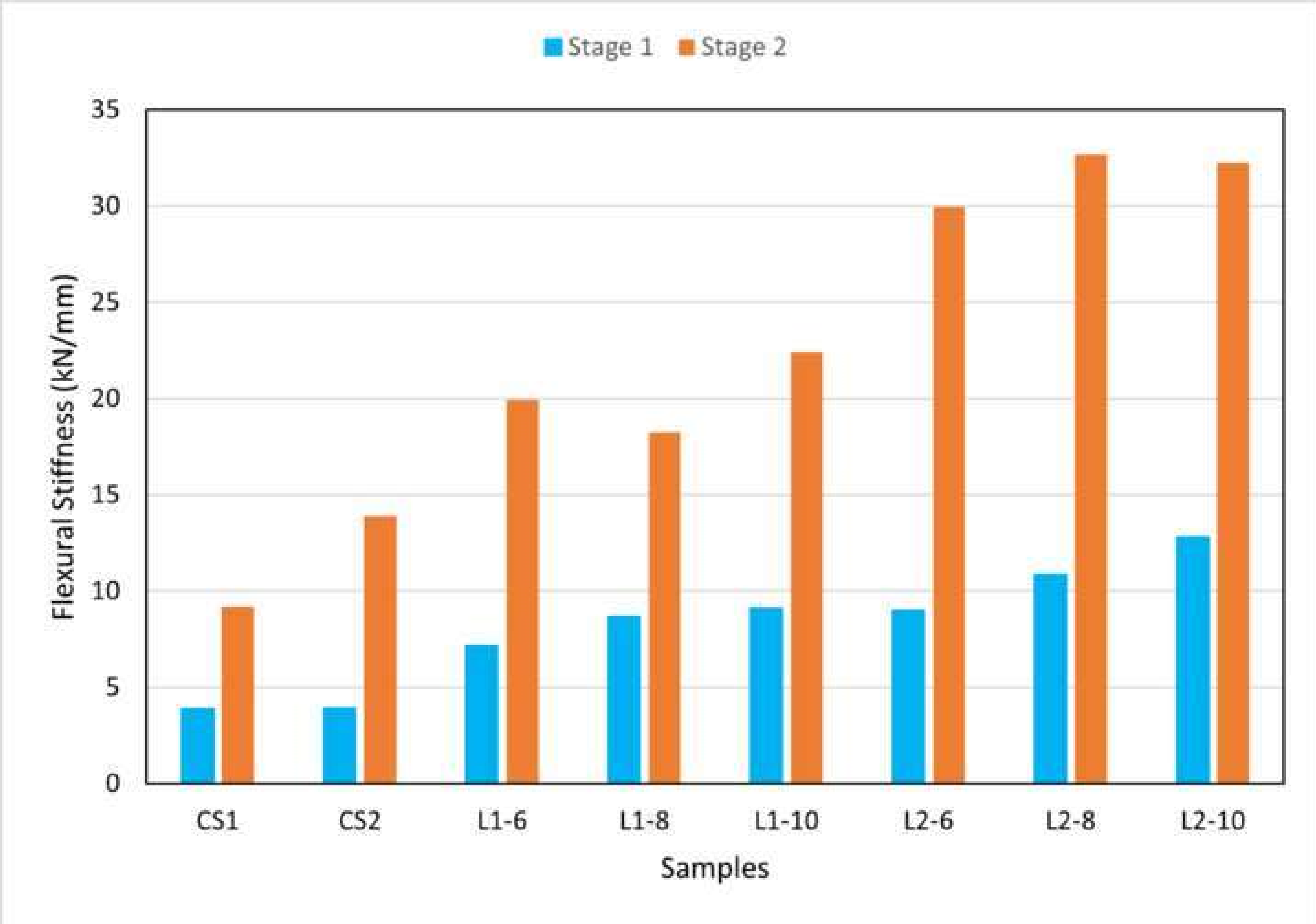
Stage 1
Stage 2
Flexural Stiffness (kN/mm)
35
30
25
20
15
10
5
0
CS1
CS2
L1-6
L1-8
L1-10
L2-6
L2-8
L2-10
Samples

Figure 12

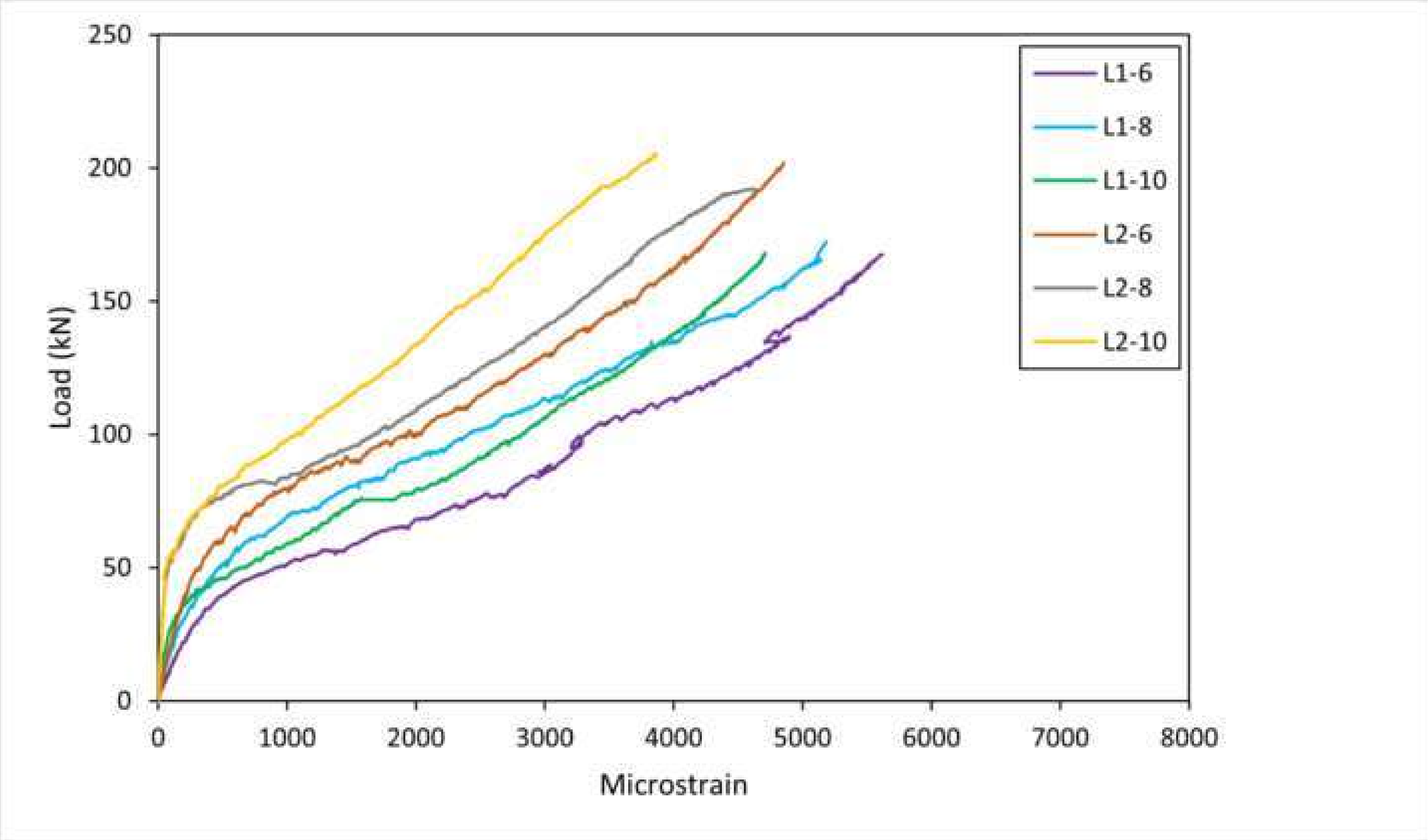
Load (kN)
250
200
150
100
50
0
0
1000
2000
3000
4000
5000
6000
7000
8000
Microstrain
L1-6
L1-8
L1-10
L2-6
L2-8
L2-10

Figure 13

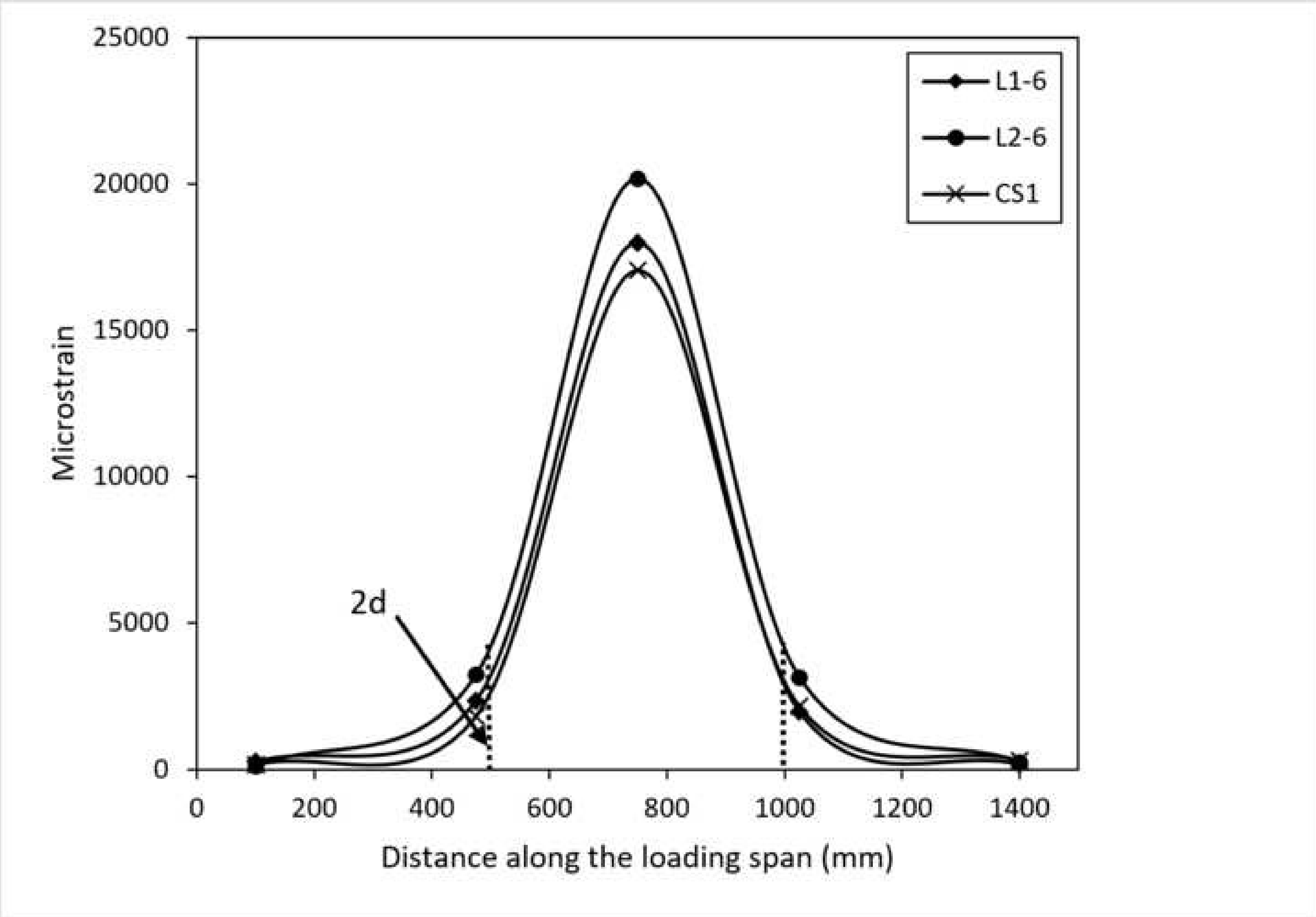

25000
20000
15000
10000
5000
0
Microstrain
0
200
400
600
800
1000
1200
1400
Distance along the loading span (mm)
2d
L1-6
L2-6
CS1

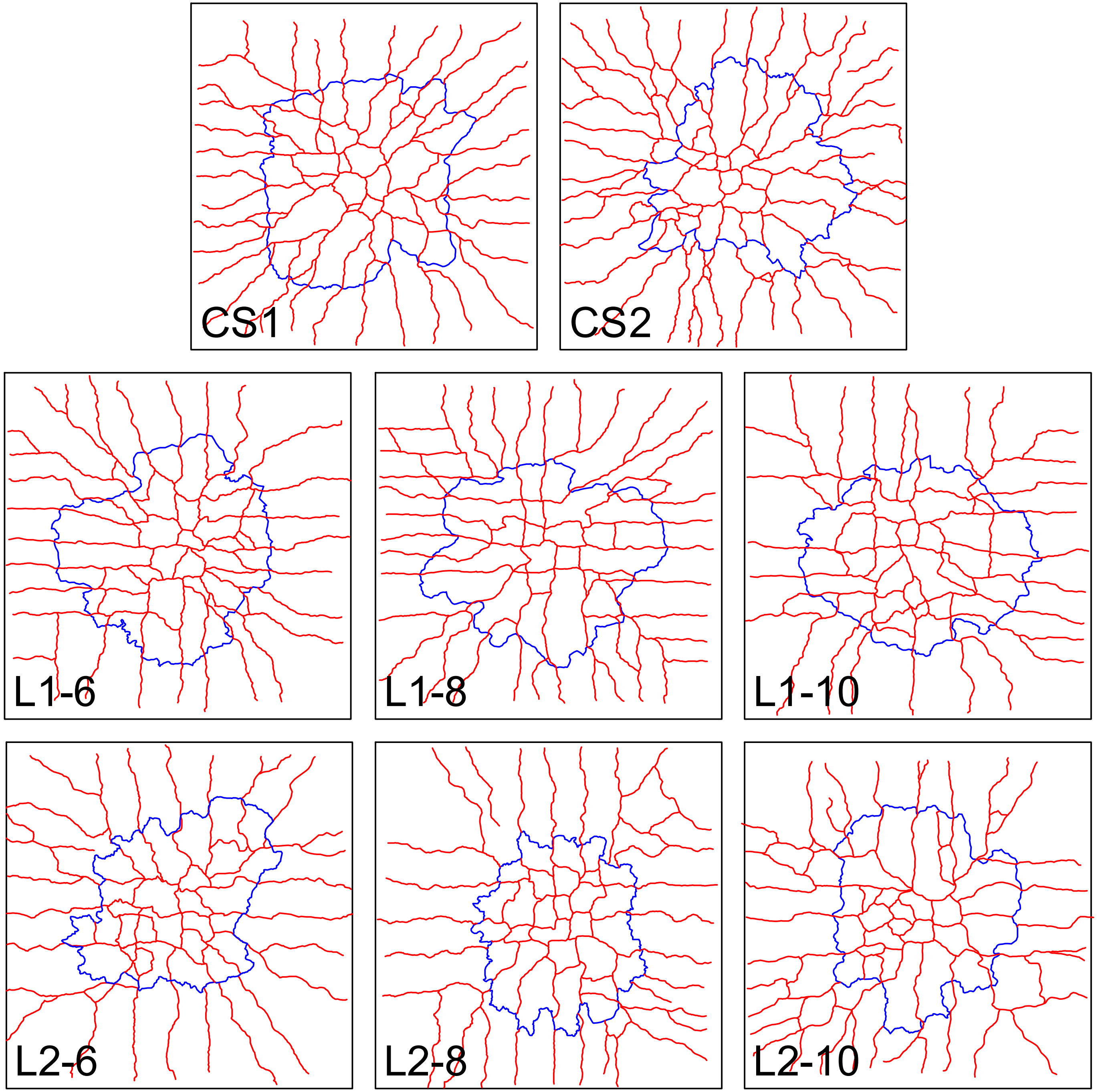
CS1
CS2
L1-6
L1-8
L1-10
L2-6
L2-8
L2-10

Figure 15

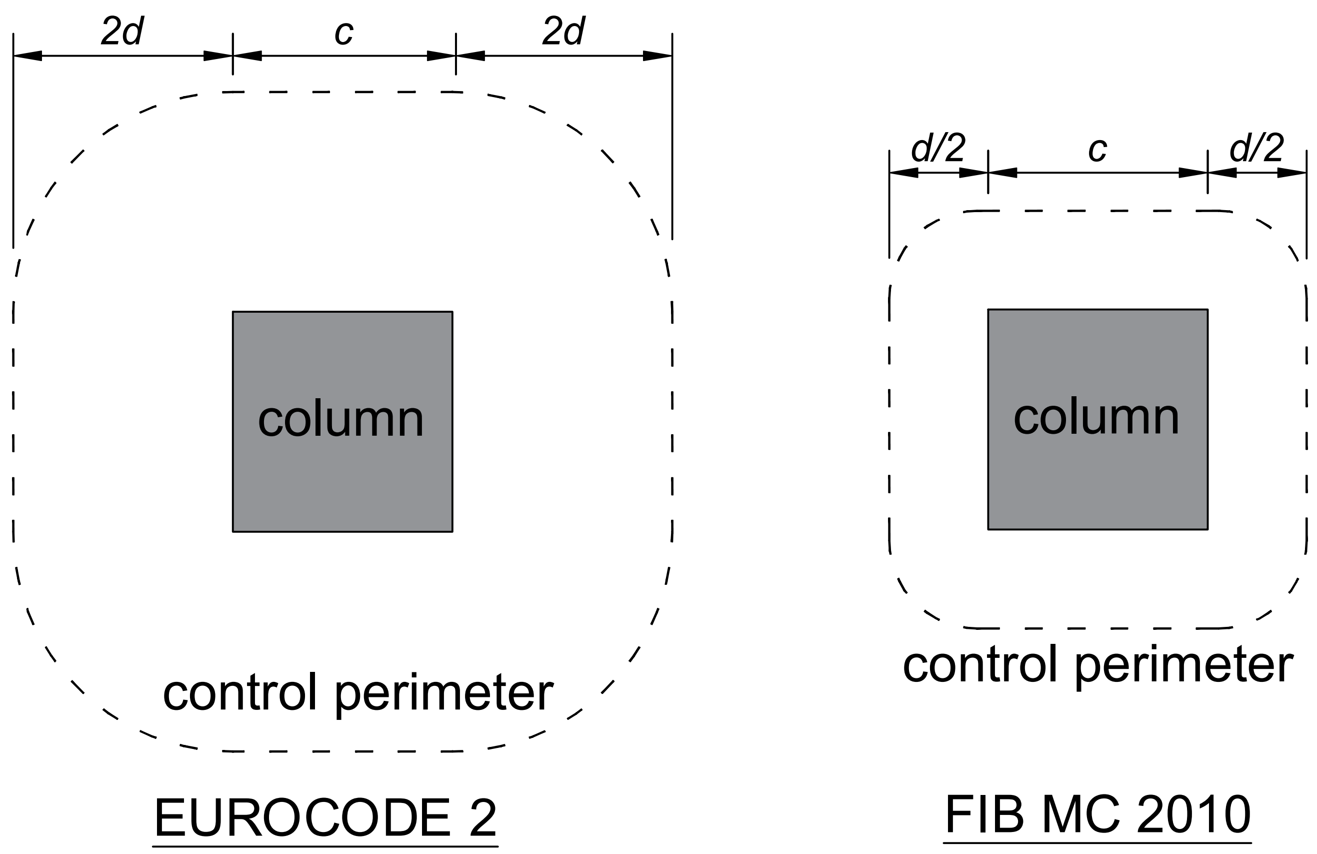
2d
c
2d
column
control perimeter
EUROCODE 2
d/2
c
d/2
column
control perimeter
FIB MC 2010

Figure 16

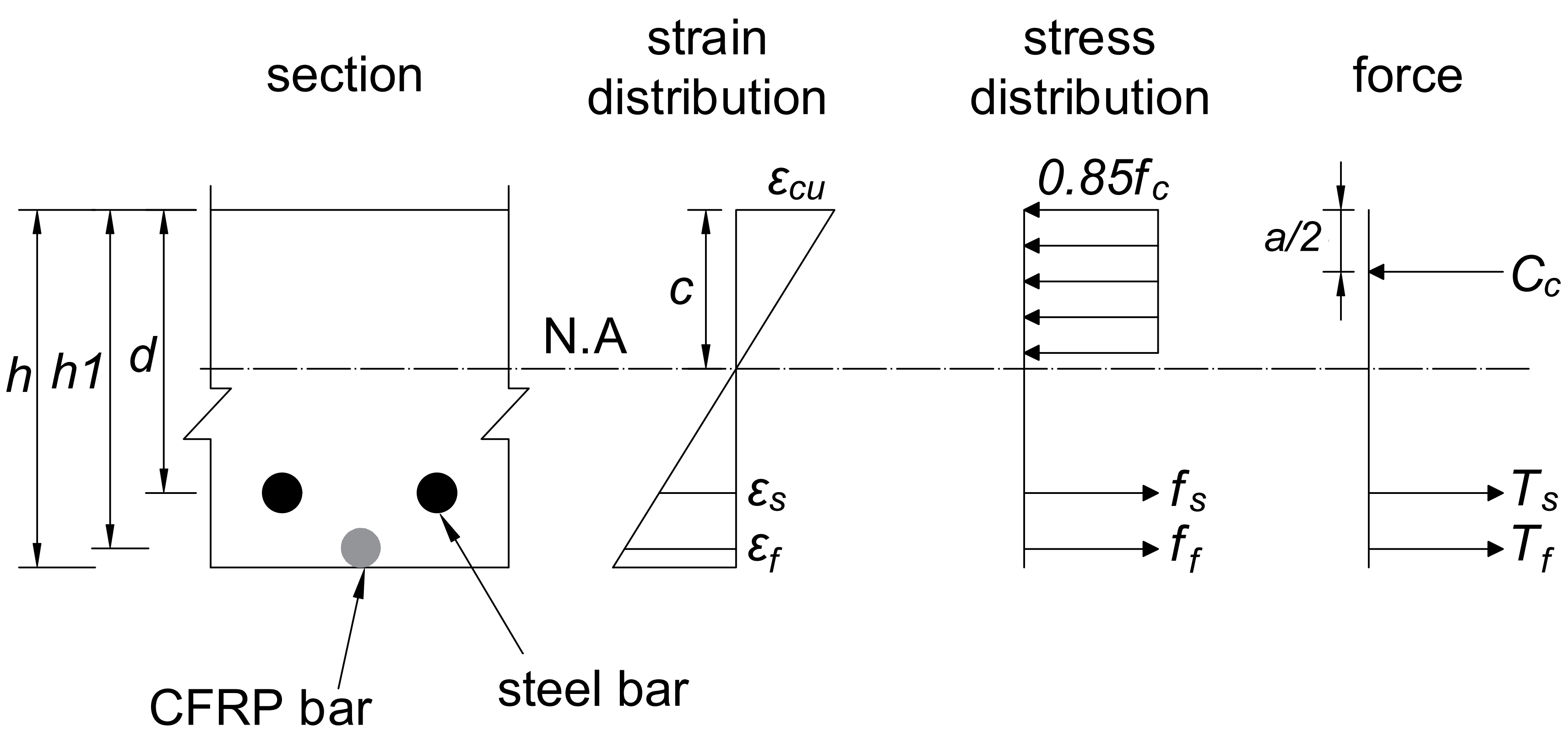
section
strain distribution
stress distribution
force
h
h1
d
N.A
c
εcu
εs
εf
0.85fc
fs
ff
a/2
Cc
Ts
Tf
CFRP bar
steel bar

Figure 17

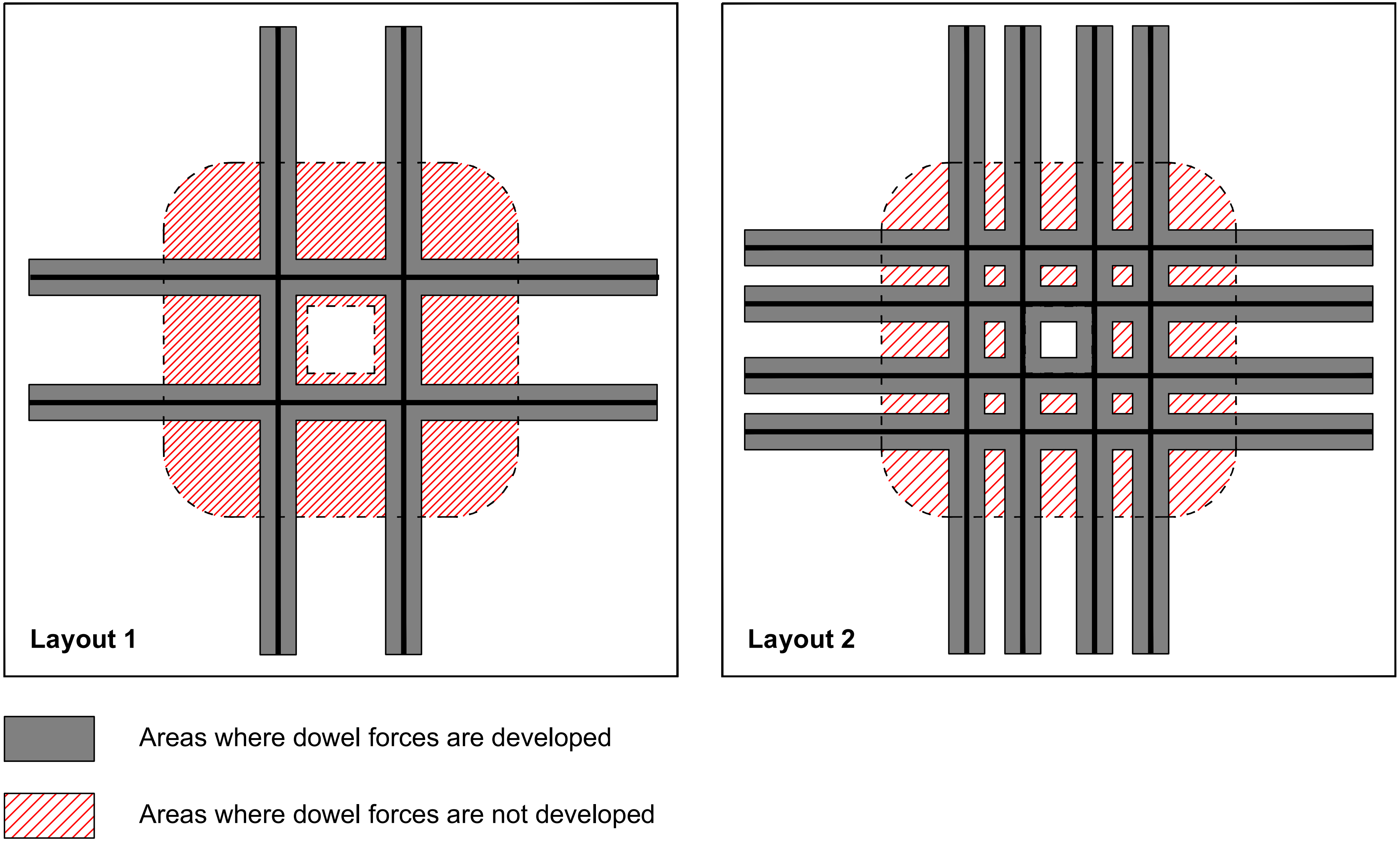
Layout 1
Layout 2
Areas where dowel forces are developed
Areas where dowel forces are not developed